

# Revision of the $^{15}\text{N}(p,\gamma)^{16}\text{O}$ reaction rate and oxygen abundance in H–burning zones

A. Caciolli<sup>1,2</sup>, C. Mazzocchi<sup>\*3</sup>, V. Capogrosso<sup>3</sup>, D. Bemmerer<sup>4</sup>, C. Broggini<sup>1</sup>, P. Corvisiero<sup>5</sup>, H. Costantini<sup>5</sup>, Z. Elekes<sup>6</sup>, A. Formicola<sup>7</sup>, Zs. Fülöp<sup>6</sup>, G. Gervino<sup>8</sup>, A. Guglielmetti<sup>3</sup>, C. Gustavino<sup>7</sup>, Gy. Gyürky<sup>6</sup>, G. Imbriani<sup>9</sup>, M. Junker<sup>7</sup>, A. Lemut<sup>\*\*5</sup>, M. Marta<sup>\*\*\*4</sup>, R. Menegazzo<sup>1</sup>, S. Palmerini<sup>10</sup>, P. Prati<sup>5</sup>, V. Roca<sup>9</sup>, C. Rolfs<sup>11</sup>, C. Rossi Alvarez<sup>1</sup>, E. Somorjai<sup>6</sup>, O. Straniero<sup>12</sup>, F. Strieder<sup>11</sup>, F. Terrasi<sup>13</sup>, H. P. Trautvetter<sup>11</sup>, and A. Vomiero<sup>14</sup>

<sup>1</sup> Istituto Nazionale di Fisica Nucleare (INFN), Sezione di Padova, via Marzolo 8, I–35131 Padova, Italy

<sup>2</sup> Dipartimento di Scienze della Terra, Università di Siena, I–53100 Siena, and Centro di GeoTecnologie CGT, I–52027 San Giovanni Valdarno, Italy

<sup>3</sup> Università degli Studi di Milano and INFN, Sezione di Milano, I–20133 Milano, Italy

<sup>4</sup> Helmholtz–Zentrum Dresden–Rossendorf, Bautzner Landstr. 400, 01328 Dresden, Germany

<sup>5</sup> Università di Genova and INFN Sezione di Genova, Genova, I–16146 Genova, Italy

<sup>6</sup> Institute of Nuclear Research (ATOMKI), H–4026 Debrecen, Hungary

<sup>7</sup> INFN, Laboratori Nazionali del Gran Sasso (LNGS), I–67010 Assergi (AQ), Italy

<sup>8</sup> Dipartimento di Fisica Sperimentale, Università di Torino and INFN Sezione di Torino, I–10125 Torino, Italy

<sup>9</sup> Dipartimento di Scienze Fisiche, Università di Napoli Federico II, and INFN Sezione di Napoli, I–80126 Napoli, Italy

<sup>10</sup> Dipartimento di Fisica, Università degli studi di Perugia and INFN, Sezione di Perugia, I–06123, Perugia Italy

<sup>11</sup> Institut für Experimentalphysik, Ruhr–Universität Bochum, D–44780 Bochum, Germany

<sup>12</sup> INAF–Osservatorio Astronomico di Collurania, I–64100 Teramo, Italy

<sup>13</sup> Seconda Università di Napoli, I–81100 Caserta, and INFN Sezione di Napoli, I–80126 Napoli, Italy

<sup>14</sup> CNR IDASC SENSOR Lab and Dipartimento di Chimica e Fisica per l’Ingegneria e per i Materiali, Università di Brescia, Brescia, Italy

Preprint online version: August 9, 2018

## ABSTRACT

**Context.** The NO cycle takes place in the deepest layer of a H–burning core or shell, when the temperature exceeds  $T \simeq 30 \cdot 10^6$  K. The O depletion observed in some globular cluster giant stars, always associated with a Na enhancement, may be due to either a deep mixing during the RGB (red giant branch) phase of the star or to the pollution of the primordial gas by an early population of massive AGB (asymptotic giant branch) stars, whose chemical composition was modified by the hot bottom burning. In both cases, the NO cycle is responsible for the O depletion.

**Aims.** The activation of this cycle depends on the rate of the  $^{15}\text{N}(p,\gamma)^{16}\text{O}$  reaction. A precise evaluation of this reaction rate at temperatures as low as experienced in H–burning zones in stellar interiors is mandatory to understand the observed O abundances.

**Methods.** We present a new measurement of the  $^{15}\text{N}(p,\gamma)^{16}\text{O}$  reaction performed at LUNA covering for the first time the center of mass energy range 70–370 keV, which corresponds to stellar temperatures between  $65 \cdot 10^6$  K and  $780 \cdot 10^6$  K. This range includes the  $^{15}\text{N}(p,\gamma)^{16}\text{O}$  Gamow–peak energy of explosive H–burning taking place in the external layer of a nova and the one of the hot bottom burning (HBB) nucleosynthesis occurring in massive AGB stars.

**Results.** With the present data, we are also able to confirm the result of the previous R–matrix extrapolation. In particular, in the temperature range of astrophysical interest, the new rate is about a factor of 2 smaller than reported in the widely adopted compilation of reaction rates (NACRE or CF88) and the uncertainty is now reduced down to the 10% level.

**Key words.** physical data and processes: nuclear reactions, abundances

## 1. Introduction

Hydrogen burning in stars proceeds through two different sets of nuclear reactions: the proton proton (pp) chain and the carbon nitrogen oxygen (CNO) cycle. While in low mass main sequence

stars the energy supply is provided by the pp–chain<sup>1</sup>, the CNO cycle is the principal nuclear process in the core of high mass main sequence stars ( $M \gtrsim 1.2 M_{\odot}$ ) as well as in the H–burning shell of giant stars Iben(1967). Furthermore, a hot CNO cycle may occur at the surface of H–accreting compact objects, like white dwarfs or neutron stars Jose & Hernanz(1998).

The set of nuclear reactions involved in the CNO cycle is illustrated in Fig. 1. Actually, it is a combination of two distinct cycles, called CN and NO, respectively. The proton capture on  $^{15}\text{N}$  results in two possible channels, the  $^{15}\text{N}(p,\alpha)^{12}\text{C}$

\* present address: Inst. of Experimental Physics University of Warsaw ul. Hoza 69 00–682 Warszawa, Poland

\*\* present address: Nuclear Science Division, Lawrence Berkeley National Laboratory, 1 Cyclotron Rd MS 88–R0192, Berkeley, CA 94720–8101, USA

\*\*\* present address: GSI Helmholtzzentrum für Schwerionenforschung, 64291 Darmstadt, Germany

<sup>1</sup> The pp–chain also dominates the H burning in extremely–metal–poor stars of any mass, due to the lack of C, N and O nuclei

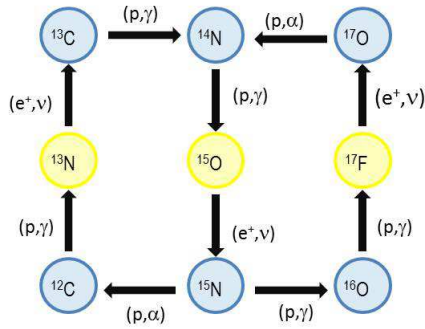


**Fig. 1.** The CNO bi–cycle.

and the  $^{15}\text{N}(p,\gamma)^{16}\text{O}$ , respectively: the ratio of the rates provides the linkage between the CN and the NO cycles. The CN cycle becomes fully active when the temperature attains  $T_9 \gtrsim 0.016\text{--}0.020^2$ , while the NO cycle requires higher temperatures ( $T_9 \gtrsim 0.030\text{--}0.035^3$ ). In case of an active NO cycle, this process determines the abundances of all the stable oxygen isotopes ( $^{16}\text{O}$ ,  $^{17}\text{O}$ ,  $^{18}\text{O}$ ). For this reason, a precise evaluation of the  $^{15}\text{N}(p,\gamma)^{16}\text{O}$  reaction rate is needed to address several astrophysical problems, like deep mixing scenarios in red giant stars, see e.g. [sweigart1979, langer1986, charb98, kraft93, boo95, wass95, denis2003, pal10, hot bottom burning nucleosynthesis in massive AGB stars Renzini & Voli(1981) or the H–burning nucleosynthesis in nova–like events Iliadis et al.(2002), Jose et al.(2007).

At low energies the cross section  $\sigma(E)$  of the  $^{15}\text{N}(p,\gamma)^{16}\text{O}$  reaction ( $Q$ –value = 12.127 MeV) is typically expressed in terms of the astrophysical  $S$ –factor  $S(E)$  defined for this reaction as:

$$S(E) = \sigma(E)E \exp(212.85/\sqrt{E}) \quad (1)$$

where  $E$  is the center of mass energy in keV.

In hydrostatic H–burning, the Gamow peak energy of this reaction ranges between 30 and 100 keV. Larger values, up to 300 keV, may be attained during explosive burning. In this energy range, the astrophysical  $S$ –factor is influenced by two resonances at  $E = 312$  and  $964$  keV<sup>4</sup> related to excited states in  $^{16}\text{O}$  at  $E_x = 12440$  and  $13090$  keV, respectively. The reaction rates reported in the NACRE Angulo et al.(1999) and the CF88 Caughlan & Fowler(1988) compilations are based on the direct measurement presented by Rolfs and Rodney (1974). However, more recent R–matrix studies Mukhamedzhanov et al.(2008), Barker(2008), which also take into account a previous ANC measurement Mukhamedzhanov et al.(2008), suggested a substantial reduction of the  $S(0)$  (i.e. the astrophysical factor at  $E = 0$ ). This result is in agreement with older direct measurements Hebbard(1960), Brochard et al.(1973).

This discrepancy prompted an in–depth study of the reaction at LUNA (Laboratory for Underground Nuclear Astrophysics). The LUNA facility has been designed to study nuclear reactions of astrophysical interest at the same energies of the stellar interiors, by taking advantage of the ultra–low background Bemmerer et al.(2005), Caciolli et al.(2009) of the

INFN–Gran Sasso underground laboratory (a detailed description of LUNA and its experimental study of the pp chain and CNO cycle may be found in the following reviews: Costantini et al.(2009), Brogini et al.(2010)). First of all, a re–analysis of data taken with nitrogen gas target of natural isotopic composition (0.4%  $^{15}\text{N}$ ) at  $E = 90\text{--}230$  keV has been performed Bemmerer et al.(2009). Then, a new measurement has been carried out at LUNA and Notre Dame LeBlanc et al.(2010). HPGe detectors and enriched TiN solid targets have been used to cover a wide energy range, namely:  $E = 120\text{--}1800$  keV. Although the minimum energy is still too high to study most of the stellar H–burning environments, thanks to the excellent accuracy (7%) and the wide energy range, this new experiment provided a dataset suitable for an R–matrix extrapolation toward lower energies.

In this paper, we present a third experiment performed at LUNA, designed to explore lower energies. The use a BGO detector, having a higher  $\gamma$ –detection efficiency compared to the HPGe detectors, allowed us to easily cover the 312 keV resonance region and to extend the direct measurements down to 70 keV. The aim of this further effort is twofold. First of all, the new data set covers the Gamow peak corresponding to the explosive burning in Novae as well as hot bottom burning in massive AGB stars. Furthermore, it provides an independent test of the low energy R–matrix extrapolation.

In the next section we illustrate the experiment, the data analysis and the results. In particular, a comparison of the present, independent measurement with the low energy predictions of the R–matrix analysis LeBlanc et al.(2010), leads to the conclusion that the  $^{15}\text{N}(p,\gamma)^{16}\text{O}$  reaction rate is now known within a 10% confidence interval. A summary of the astrophysical studies requiring an accurate evaluation of the  $^{15}\text{N}(p,\gamma)^{16}\text{O}$  reaction rate follows.

## 2. The new underground experiment

The target and the  $\gamma$ –ray detection set–up are those used in previous measurements and have been already extensively described elsewhere (for instance see Limata et al.(2010)). The proton beam (30–150  $\mu\text{A}$ ) reaches the water cooled target after passing a 5 mm diameter collimator and a 1 m long copper tube, which is cooled to liquid nitrogen temperatures and works as a cold trap in order to prevent impurities scattered by the beam from depositing on the target surface. The pressure in the target chamber is  $5 \cdot 10^{-7}$  mbar and no carbon deposition on the target is observed after the irradiation. This is checked by performing scans of the profile of the  $^{14}\text{N}(p,\gamma)^{15}\text{O}$  resonance at  $E_p = 278$  keV. The target chamber works as a Faraday cup and provides the integral of the charge deposited, hence the average beam intensity, with an overall uncertainty of 2% (a  $\sim 300$  V high voltage is applied to the cold trap to suppress the secondary electron emission).

The target is surrounded by a  $4\pi$ –BGO summing crystal (28 cm long, 20 cm diameter, and 6 cm coaxial hole, Casella et al.(2002)). The  $4\pi$ –BGO is essential in order to increase the  $\gamma$ –detection efficiency, which is calculated with a simulation based on GEANT4 Agostinelli et al.(2003) and carefully checked with radioactive sources and with the  $\gamma$ –ray produced by the proton induced reaction  $^{11}\text{B}(p,\gamma)^{12}\text{C}$  at the  $E = 149$  keV resonance. The simulation needs experimental inputs, such as the decay scheme and the angular distribution of the emitted  $\gamma$ –radiation. The decay branching ratios for transitions to the excited state of  $^{16}\text{O}$  have been measured by Rolfs and Rodney (1974), Bemmerer et al. (2009) and LeBlanc et al. (2010). The angular distribution has been found to be isotropic in a previous

<sup>2</sup>  $T_9 = T(K)/10^9$ .

<sup>3</sup> The activation temperatures of both the CN and the NO cycles depend on the actual amount of C, N and O nuclei and, therefore, on the stellar metallicity.

<sup>4</sup> In the center of mass reference. Beam energies are given in the center of mass reference unless otherwise stated

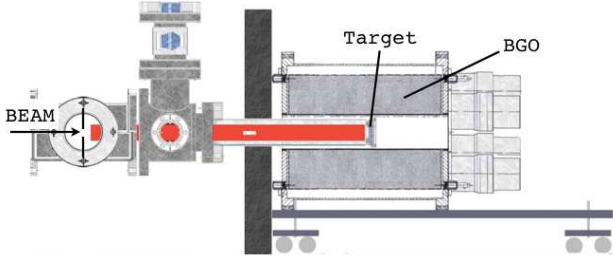


**Fig. 2.** Schematic representation of the last portion of the beam–line with the detection set–up.

LUNA work LeBlanc et al.(2010). By considering all the contributions described above in the simulation code, the total uncertainty on the efficiency is 3%.

The TiN forming the target material, enriched in  $^{15}\text{N}$ , is deposited on a tantalum backing with the reactive sputtering technique Rigato et al.(2001). The target thickness is 100 nm, as verified through secondary neutral mass spectroscopy Vad et al.(2009) (the uncertainty on this measurement is included in the contribution to the target analysis in Table 2), corresponding to 15 keV energy loss at  $E = 259$  keV. The stoichiometry Ti/N, which ranges from 0.97 to 1.18 according to the target, is measured for each target with the high Z elastic recoil detection (ERD) technique Bergmaier et al.(1998). Isotopic abundances between 96% and 99%, according to the target, are deduced from the observed height of the plateau in the yield of the  $^{14}\text{N}(p,\gamma)^{15}\text{O}$  resonance at  $E = 259$  keV, and from the ERD data. The results from these two methods agree within 2%. Finally, the target deterioration, caused by the impinging high–intensity proton beam has been studied by using the 430 keV resonance of  $^{15}\text{N}(p,\alpha\gamma)^{12}\text{C}$  Marta et al.(2010). The targets have been analyzed by looking at the shape of the plateau in the yield distribution for the 430 keV resonance. The surface irradiated by the LUNA beam and the area outside the LUNA beam–spot are investigated, so that appropriate corrections for the target deterioration during measurements are derived.

The laboratory background in the  $^{15}\text{N}(p,\gamma)^{16}\text{O}$  region of interest is about 6 counts/day. The beam induced background in the same region, produced by the  $^{11}\text{B}(p,\gamma)^{12}\text{C}$  reaction, is monitored by means of the peak produced by this reaction at 16.1 MeV (see Fig. 3 as an example of the acquired spectra). The counts in this peak are usually more than in the 11 MeV peak produced by the same reaction, which lies within the  $^{15}\text{N}(p,\gamma)^{16}\text{O}$  region of interest of the spectrum Bemmerer et al.(2009). We have rejected all measurements where the 16 MeV peak contained more than 3% of the counts in our region of interest.

The target profiles can be integrated with the cross section in order to calculate the expected yield as:

$$Y_{sim} = \int_{x_0}^{x_{max}} S(E_p) \cdot E_p \exp\left(\frac{212.85}{\sqrt{E_p}}\right) \eta_{BGO} \cdot n_{target}(x) \frac{^{15}\text{N}}{\text{N}} dx \quad (2)$$

where  $E_p$  is the energy in the laboratory system expressed in keV and it depends on the beam position  $x$  along the target thickness,  $\eta_{BGO}$  is the efficiency, and  $n_{target}(x) \frac{^{15}\text{N}}{\text{N}}$  is the number of  $^{15}\text{N}$  nuclides in the  $x$  position in the target. By comparing the experimental yield  $Y_{exp}$  with the calculated one, it is possible to determine the S–factor as follows:

$$S(E_{eff})_{exp} = \frac{Y_{exp}}{Y_{sim}} \cdot S(E_{eff})_{th} \quad (3)$$

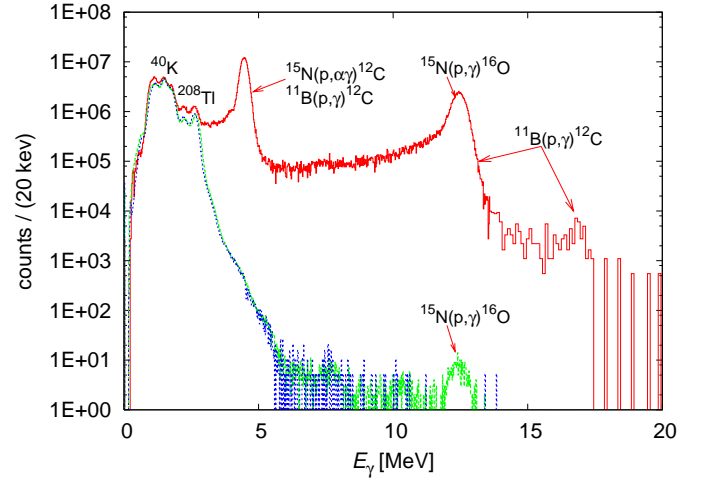


**Fig. 3.** Spectra taken at  $E_p = 330$  keV (red),  $E_p = 80$  keV (green), and laboratory background spectrum (blue), normalized to the same time.

**Table 1.** The absolute S–factor data and their statistical uncertainties from the present work. The systematic error is 11%.

| $E$<br>[keV] | $S$<br>[keV barn] | $\Delta S^{stat}$<br>[keV barn] | $E$<br>[keV] | $S$<br>[keV barn] | $\Delta S^{stat}$<br>[keV barn] |
|--------------|-------------------|---------------------------------|--------------|-------------------|---------------------------------|
| 72.8         | 52                | 4                               | 236.9        | 153.0             | 1.1                             |
| 81.3         | 49                | 2                               | 246.3        | 172.0             | 1.7                             |
| 89.3         | 53                | 6                               | 256.4        | 201               | 3                               |
| 105.1        | 59                | 4                               | 266.3        | 227               | 3                               |
| 114.8        | 53                | 3                               | 274.5        | 254.7             | 1.4                             |
| 123.5        | 56.4              | 1.8                             | 283.5        | 283               | 3                               |
| 132.7        | 64                | 2                               | 293.7        | 315.4             | 1.6                             |
| 143.7        | 68.3              | 1.0                             | 302.6        | 320               | 2                               |
| 151.3        | 55.9              | 1.1                             | 311.7        | 309.1             | 1.2                             |
| 162.3        | 79.2              | 0.5                             | 321.1        | 277.6             | 1.0                             |
| 170.7        | 79.8              | 0.9                             | 330.4        | 227.4             | 0.7                             |
| 180.1        | 87.2              | 1.0                             | 340.2        | 183.0             | 0.9                             |
| 189.1        | 93.5              | 1.1                             | 349.1        | 134.0             | 0.9                             |
| 198.4        | 102.6             | 0.8                             | 354.1        | 124.0             | 1.2                             |
| 207.9        | 114.0             | 1.6                             | 358.8        | 101.0             | 1.0                             |
| 217.3        | 123.0             | 1.0                             | 363.6        | 95.1              | 0.9                             |
| 227.4        | 136.0             | 1.1                             | 368.3        | 81.0              | 0.8                             |

where the effective energy is calculated according to the following definition Lemut(2008):

$$E_{eff} = \frac{\int_{x_0}^{x_{max}} S(E) \cdot E \exp\left(\frac{212.85}{\sqrt{E}}\right) \cdot n_{target}(x) \cdot \frac{^{15}\text{N}}{\text{N}} \cdot E \cdot dx}{\int_{x_0}^{x_{max}} S(E) \cdot E \exp\left(\frac{212.85}{\sqrt{E}}\right) \cdot n_{target}(x) \cdot \frac{^{15}\text{N}}{\text{N}} dx} \quad (4)$$

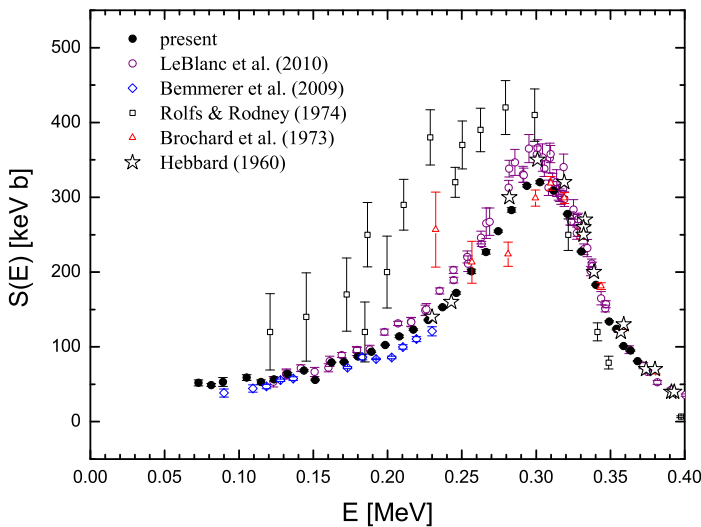
In Eq. (4) the theoretical S–factor is used. Four different theoretical S–factors are considered in Eq. (2) and Eq. (4): the one reported in LeBlanc et al.(2010) and the one reported in Mukhamedzhanov et al.(2011), a constant S–factor and a value obtained from a recursive analysis process. In all cases, the same results are obtained within 1% discrepancies which is included in the error on the effective energy.

As reported in Table 1, the  $^{15}\text{N}(p,\gamma)^{16}\text{O}$  astrophysical S–factor is obtained for the center of mass energy range 70–370 KeV. The statistical uncertainty is always limited within a few percent, reaching a maximum value of 10% at  $E = 72.8$  keV. All sources of systematic uncertainties are given in Table 2 and sum to a total systematic uncertainty of 10%.

**Table 2.** S–factor systematic uncertainties.

| Source description                                | Estimated uncertainty |
|---|-----------------------|
| Target analysis                                   | 7.5%                  |
| stopping power                                    | 4.0%                  |
| $^{15}\text{N}$ isotopic ratio                    | 2.0%                  |
| Ti/N stoichiometry                                | 2.0%                  |
| Beam intensity                                    | 2.0%                  |
| Effective energy                                  | 3.0%                  |
| $\gamma$ –ray detection efficiency                | 3.0 %                 |
| $^{11}\text{B}(p,\gamma)^{12}\text{C}$ background | 3.0%                  |
| Total systematic uncertainty                      | 10.0%                 |

A comparison of the derived astrophysical S–factor to the results of previous experiments is shown in Fig. 4. We confirm the

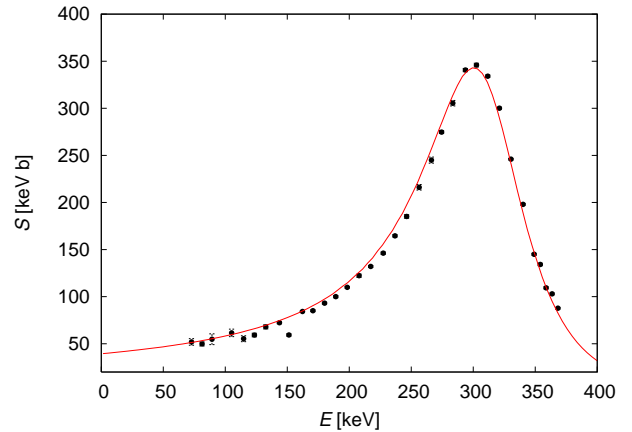
**Fig. 4.** The S–factor as a function of energy. Present data (black dots) are compared to the results of previous experiments.

previous finding concerning the need of a substantial reduction of the  $S(0)$  value. The present result is significantly lower than the resonant cross section from Rolfs and Rodney (1974), i.e. the data set adopted in NACRE and CF88, and, by considering the systematic uncertainty, in good agreement with our previous HPGe measurement LeBlanc et al.(2010). In particular, according to the present absolute analysis, the cross section on top of the  $E = 312$  keV resonance is  $\sigma(312 \text{ keV}) = 6.0 \pm 0.6 \mu\text{b}$ , where the quoted error includes the 10 % systematic uncertainty. In Table 3, we compare this result to the values of previous measurements. The weighted average of 3 measurements<sup>5</sup> leads to a recommended value of  $\bar{\sigma}(312 \text{ keV}) = 6.5 \pm 0.3 \mu\text{b}$ . The shape of the R–Matrix fit has been also compared to the present data as shown in Fig. 5. Only for this comparison the present data have been corrected for the electron screening in the adiabatic approximation Assenbaum et al.(1987) (at most 10% at 70 keV) and they have been rescaled to the calculated average value. This rescaling is still within the systematic uncertainties of the present absolute data. They show an excellent agreement with the energy dependence of the LUNA R–Matrix fit LeBlanc et al.(2010).

<sup>5</sup> The result obtained by Brochard et al.(1973) has been excluded, because no uncertainty was reported.

**Table 3.** Summary of 312 keV resonance cross sections in comparison to previous results (see text for details and references). The uncertainty reported by Hebbard (1960) has been obtained by assuming it to be 10% as reported by Barker(2008).

| Present study [ $\mu\text{b}$ ] | LeBlanc <i>et al.</i> [ $\mu\text{b}$ ] | Rolfs and Rodney [ $\mu\text{b}$ ] | Brochard <i>et al.</i> [ $\mu\text{b}$ ] | Hebbard [ $\mu\text{b}$ ] |
|---------------------------------|---|------------------------------------|--|---------------------------|
| $6.0 \pm 0.6$                   | $6.5 \pm 0.3$                           | $9.6 \pm 1.3$                      | 6.3                                      | $6.5 \pm 0.7$             |

**Fig. 5.** The present data rescaled to the new recommended value of  $\sigma(312)$  keV (see text to details) and compared to the R–matrix predictions LeBlanc et al.(2010).

Finally, a new R–matrix analysis has been recently published by Mukhamedzhanov, La Cognata and Kroha (2011). By varying the fitting method, these authors obtain  $S(0)$  values ranging between 33.1 and 40.1 keVb, which is in excellent agreement with the value reported by LeBlanc et al. ( $S(0) = 39.6 \pm 2.6$  keVb).

For practical purposes, the nuclear reaction rate can be approximated by the following fitting formula LeBlanc et al.(2011):

$$N_A \langle \sigma v \rangle = a_1 10^9 T^{-\frac{2}{3}} \exp[a_2 T^{-\frac{1}{3}} - (T/a_3)^2] [1 + a_4 T + a_5 T^2] + a_6 10^3 T^{-\frac{3}{2}} \exp(a_7/T) + a_8 10^6 T^{-\frac{3}{2}} \exp(a_9/T), \quad (5)$$

where the best fit parameters are reported in Table 4.

**Table 4.** Best fit parameters for the  $^{15}\text{N}(p,\gamma)^{16}\text{O}$  reaction rate given in LeBlanc et al.(2010).

|                 |                |                |
|-----------------|----------------|----------------|
| $a_1 = 0.523$   | $a_4 = 6.339$  | $a_7 = -2.913$ |
| $a_2 = -15.240$ | $a_5 = -2.164$ | $a_8 = 3.048$  |
| $a_3 = 0.866$   | $a_6 = 0.738$  | $a_9 = -9.884$ |

### 3. Summary and Conclusions

In this paper we have discussed the experimental efforts done to improve our knowledge of the  $^{15}\text{N}(p,\gamma)^{16}\text{O}$  reaction rate in the temperature range experienced by any H–burning zone in stellar



interiors. Such an important reaction is located at the branching point between the CN and NO cycles. The branching ratio, as a function of the temperature, is shown in Fig. 6, where the solid line has been obtained by means of the widely adopted reaction rate given by NACRE, while the dashed line represents the revised scenario as derived from the latest R-matrix study (see section 2). In both cases, the rate suggested by NACRE has

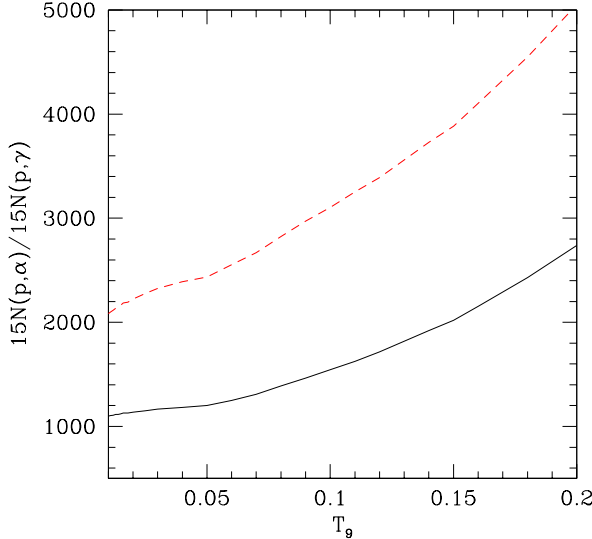


**Fig. 6.** The CN–NO branching ratio, as a function of the temperature, under different assumptions for the  $^{15}\text{N}(p,\gamma)^{16}\text{O}$  reaction rate: NACRE (solid line) and the revised rate (dashed line).

been used for the competitive  $^{15}\text{N}(p,\alpha)^{12}\text{C}$  reaction<sup>6</sup>. A look at the solid line shows that in the whole range of temperatures experienced by the core and the shell–H burning, the  $\alpha$ -channel is between 1000 to 2000 times more efficient than the  $\gamma$  channel: just 1 to 2 protons out of every 2000 are consumed by the NO cycle. When the updated rate for the  $^{15}\text{N}(p,\gamma)^{16}\text{O}$  is adopted, such a ratio becomes about a factor of 2 larger. Although such a variation has negligible consequences on the overall nuclear energy production, a change in the rate of the  $^{15}\text{N}(p,\gamma)^{16}\text{O}$  affects the equilibrium abundances of the stable oxygen isotopes within the H burning zone. As an example, the equilibrium abundance of  $^{16}\text{O}$  is reported as a function of the temperature in Fig. 7. Also in this case, the solid and the dashed lines represent the values obtained by adopting the NACRE and the revised rate of the  $^{15}\text{N}(p,\gamma)^{16}\text{O}$  reaction, respectively.

Let us point out that the most important improvement resulting from the present analysis of the CN–NO branching concerns the significant reduction of the nuclear physics uncertainties, other than the change of the reaction rate with respect to the values reported by CF88 or NACRE. For stellar models and nucleosynthesis calculations implying H-burning whose Gamow peak energy is larger than the minimum value attained by the LUNA BGO experiment, namely  $E_0 > 70$  KeV, which corresponds to a temperature  $T > 65 \cdot 10^6$  K, a true experimental error (smaller than 10%) is now available for this important reaction rate. Note that only in a very few cases the reaction rate

<sup>6</sup> This reaction has been recently studied with the THM method Cognata et al.(2009). The authors do not report a reaction rate but only the  $S(0)$  value. Scaling the previous NACRE results on that value the following considerations do not change so we still adopt the NACRE results in the present work

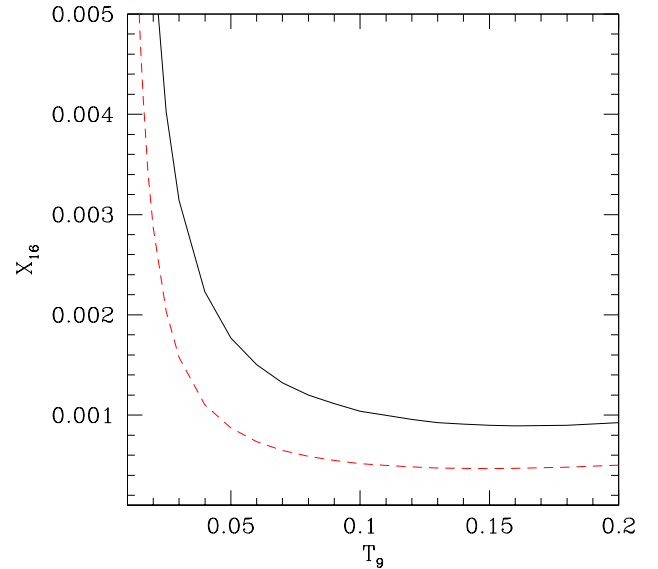


**Fig. 7.** The  $^{16}\text{O}$  equilibrium abundance (mass fraction) as given by:  $X_{16} = X_{15} \frac{16}{15} \frac{\langle \sigma v \rangle_{^{15}\text{N}+p}}{\langle \sigma v \rangle_{^{16}\text{O}+p}}$ . The solid and the dashed lines represents the old (NACRE) and the new (revised) prescriptions for the  $^{15}\text{N}(p,\gamma)^{16}\text{O}$  reaction rate. A solar  $^{15}\text{N}$  mass fraction ( $X_{15}$ ), as derived by Asplund et al. 2010, has been used. In both cases, NACRE prescriptions for the  $\langle \sigma v \rangle_{^{16}\text{O}+p}$  have been adopted.

has been measured down to the stellar Gamow peak energy (see, e.g., Bonetti et al.(1999)). In addition, basing on the good agreement found between the new LUNA measurements and the revised R-matrix fit (see previous section), we are confident that the quoted small uncertainty may be assumed also in the extrapolated region.

Among the many astrophysical applications of the present analysis, we recall the explosive H-burning in Novae, which occurs at temperature larger than  $10^8$  K and, therefore, well above the achieved experimental limit. A recent study by Iliadis et al. (2002), investigates the dependence of the nova nucleosynthesis calculations on the various nuclear physics inputs. They found that a reduction of a factor of two of the  $^{15}\text{N}(p,\gamma)^{16}\text{O}$  reaction rate would imply a 30% reduction of the final oxygen abundance. Also the inner region of the convective envelope of massive AGB stars attains quite high temperature, up to  $T_9 = 0.08$ – $0.09$  (Renzini & Voli(1981), M. Forestini & C. Charbonnel(1997), D’antona & Mazzitelli(1996), Straniero et al.(2000), Lattanzio et al.(2000)). The resulting H burning, the so called hot bottom burning, coupled to the convective mixing, gives rise to a very promising nucleosynthesis scenario, where all the C, N and O isotopes are substantially affected. If the temperature is large enough ( $80 \times 10^6$  K), the Ne–Na and the Mg–Al cycles are also activated. In this context, it has been recently claimed that massive AGB stars played a fundamental role during the early evolution of globular clusters Ventura et al.(2001). According to this self-enrichment scenario, in between 50 to 100 Myr after the cluster formation, the first generation of intermediate mass stars ( $5$ – $7 M_{\odot}$ ) reached the AGB. Then, during this evolutionary phase, they underwent a substantial modification of the envelope composition, as a consequence of the HBB and several dredge up episodes. Due to the huge AGB mass loss, fresh gas enriched in He, C, N and Na, but O depleted, refilled the space occupied by the young Globular Cluster. If the star formation process was still active at that epoch, some

of the stars we observed today should show the imprint of such a delayed chemical pollution by massive AGB. In particular, the O–Na anti–correlation, as observed in Giant, sub–Giant and turn–off stars of several globular clusters ?, e.g. and reference therein]kraft1997, Carretta2009, may be the consequence of this nucleosynthesis process. Such a conclusion follows from the evidence that the temperature required for the activation of the NO cycle is similar to that required for the activation of the Ne–Na cycle. Thus, when O is depleted at the bottom of the convective envelope, Na should be enhanced. For this reason, a precise determination of the  $^{15}\text{N}(p,\gamma)^{16}\text{O}$  is one of the prerequisites to obtain a robust prediction of the O abundance and, in turn, to check the proposed self–pollution scenario for the observed O–Na anti–correlation.

The R–matrix studies also allow to extrapolate the precise experimental measurements of the  $^{15}\text{N}(p,\gamma)^{16}\text{O}$  reaction rate down to the temperature range experienced by the H–burning taking place in main sequence, RGB and less–massive AGB stars. Also in these cases the uncertainty has been significantly reduced. Such an occurrence may be immediately translated in more robust astrophysical predictions.

## Acknowledgments

We thank A. Bergmaier (Universität der Bundeswehr München) and Javier García Lopez (CNA, Centro Nacional de Aceleradores) of Seville for assistance with the isotopic abundance analysis. Financial support by INFN and in part by the European Union (TARI RII3–CT–2004– 506222, AIM 025646 and SPIRIT 227012), the Hungarian Scientific Research Fund (K68801), and DFG (BE 4100/2–1) is gratefully acknowledged.

## References

- Agostinelli, S., Allison, J., Amako, K., et al. 2003, Nuclear Instruments and Methods in Physics Research Section A: Accelerators, Spectrometers, Detectors and Associated Equipment, 506, 250
- Angulo, C., Arnould, M., Rayet, M., et al. 1999, Nuclear Physics A, 656, 3
- Assenbaum, H. J., Langanke, K., & Rolfs, C. 1987, Zeitschrift für Physik A Hadrons and Nuclei, 327, 461, 10.1007/BF01289572
- Barker, F. C. 2008, Physical Review C (Nuclear Physics), 78, 044612
- Bemmerer, D., Caciolli, A., Bonetti, R., et al. 2009, Journal of Physics G: Nuclear and Particle Physics, 36, 045202 (10pp)
- Bemmerer, D., Confortola, F., Lemut, A., et al. 2005, Eur. Phys. J. A, 24, 313
- Bergmaier, A., Dollinger, G., & Frey, C. M. 1998, Nuclear Instruments and Methods in Physics Research Section B: Beam Interactions with Materials and Atoms, 136–138, 638, ion Beam Analysis
- Bonetti, R., Brogini, C., Campajola, L., et al. 1999, Phys. Rev. Lett., 82, 5205
- Bordeanu, C., Rolfs, C., Margineanu, R., Negoita, F., & Simion, C. 2008, Journal of Physics G: Nuclear and Particle Physics, 35, 014011 (6pp)
- Brochard, F., Chevallier, P., Disdier, D., & Scheibling, F. 1973, Le Journal de Physique, 34, 363
- Brogini, C., Bemmerer, D., Guglielmetti, A., & Menegazzo, R. 2010, Annual Review of Nuclear and Particle Science, 60, 53
- Caciolli, A., Agostino, L., Bemmerer, D., et al. 2009, Eur. Phys. J. A, 39, 179
- Carretta, E., Bragaglia, A., Gratton, R. G., et al. 2009, A&A, 505, 117
- Casella, C., Costantini, H., Lemut, A., et al. 2002, Nuclear Instruments and Methods in Physics Research Section A: Accelerators, Spectrometers, Detectors and Associated Equipment, 489, 160
- Caughlan, G. R. & Fowler, W. A. 1988, Atomic Data and Nuclear Data Tables, 40, 283
- Charbonnel, C. & do Nascimento, J. D., J. 1998, A&A, 336, 915
- Cognata, M. L., Goldberg, V. Z., Mukhamedzhanov, A. M., Spitaleri, C., & Tribble, R. E. 2009, Phys. Rev. C, 80, 012801
- Costantini, H., Formicola, A., Imbriani, G., et al. 2009, Reports on Progress in Physics, 72, 086301
- D’antona, F. & Mazzitelli, I. 1996, The Astrophysical Journal, 470, 1093
- Denissenkov, P. A. & Vandenberg, D. A. 2003, The Astrophysical Journal, 593, 509
- Hebbard, D. 1960, Nuclear Physics, 15, 289
- Iben, I., J. 1967, The Astrophysical Journal, 147, 624
- Iliadis, C., Champagne, A., Jose, J., Starrfield, S., & Tupper, P. 2002, The Astrophysical Journal Supplement Series, 142, 105
- Jose, J., Garcia-Berro, E., Hernanz, M., & Gil-Pons, P. 2007, The Astrophysical Journal Letters, 662, L103
- Jose, J. & Hernanz, M. 1998, The Astrophysical Journal, 494, 680
- Kraft, R. P., Sneden, C., Langer, G. E., & Shetrone, M. D. 1993, The Astronomical Journal, 106, 1490
- Kraft, R. P., Sneden, C., Smith, G. H., et al. 1997, The Astronomical Journal, 113, 279
- Langer, G. E., Kraft, R. P., Carbon, D. F., Friel, E., & Oke, J. B. 1986, Publications of the Astronomical Society of the Pacific, 98, 473
- Lattanzio, J., Forestini, M., & Charbonnel, C. 2000, Mem. Soc. Astron. Italiana, 71, 737
- LeBlanc, P. J., Imbriani, G., Görres, J., et al. 2010, Phys. Rev. C, 82, 055804
- LeBlanc, P. J., Imbriani, G., Görres, J., et al. 2011, Phys. Rev. C, 84, 019902
- Lemut, 2008, Eur. Phys. J. A, 36, 233
- Limata, B., Strieder, F., Formicola, A., et al. 2010, Phys. Rev. C, 82, 015801
- M. Forestini & C. Charbonnel. 1997, Astron. Astrophys. Suppl. Ser., 123, 241
- Marta, M., Trompler, E., Bemmerer, D., et al. 2010, Phys. Rev. C, 81, 055807
- Mukhamedzhanov, A. M., Bém, P., Burjan, V., et al. 2008, Physical Review C (Nuclear Physics), 78, 015804
- Mukhamedzhanov, A. M., La Cognata, M., & Kroha, V. 2011, Phys. Rev. C, 83, 044604
- Palmerini, S., Cognata, M. L., Cristallo, S., & Busso, M. 2011, The Astrophysical Journal, 729, 3
- Renzini, A. & Voli, M. 1981, A&A, 94, 175
- Rigato, V., Maggioni, G., Patelli, A., et al. 2001, Surface and Coating Technology, 142–144, 943
- Straniero, O., Limongi, M., Chieffi, A., et al. 2000, Mem. Soc. Astron. Italiana, 71, 719
- Sweigart, A. V. & Mengel, J. G. 1979, The Astrophysical Journal, 229, 624
- Vad, K., Csik, A., & Langer, G. A. 2009, Spectroscopy Europe, 21, 13
- Ventura, P., D’Antona, F., Mazzitelli, I., & Gratton, R. 2001, The Astrophysical Journal Letters, 550, L65
- Wasserburg, G. J., Boothroyd, A. I., & Sackmann, I.-J. 1995, The Astrophysical Journal Letters, 447, L37